A model for p53–induced apoptosis

Article *in* Nature · October 1997

DOI: 10.1038/38525 · Source: PubMed

5 authors, including:

Kornelia Polyak
Dana-Farber Cancer Institute
410 PUBLICATIONS **75,645** CITATIONS

SEE PROFILE

Yong Xia
The Ohio State University
119 PUBLICATIONS **10,834** CITATIONS

SEE PROFILE

Bert Vogelstein
Johns Hopkins Medicine
896 PUBLICATIONS **391,444** CITATIONS

SEE PROFILE

A model for p53-induced apoptosis

Kornelia Polyak*†, Yong Xia‡, Jay L. Zweier‡, Kenneth W. Kinzler† & Bert Vogelstein*†

** The Howard Hughes Medical Institute, † The Johns Hopkins Oncology Center, 424 North Bond Street, Baltimore, Maryland 21231, USA*
‡ Division of Cardiology, Department of Medicine, Johns Hopkins University School of Medicine, Baltimore, Maryland 21205, USA

The inactivation of the *p53* gene in a large proportion of human cancers has inspired an intense search for the encoded protein's physiological and biological properties. Expression of p53 induces either a stable growth arrest or programmed cell death (apoptosis). In human colorectal cancers, the growth arrest is dependent on the transcriptional induction of the protein $p21^{WAF1/CIP1}$ (ref. 1), but the mechanisms underlying the development of p53-dependent apoptosis are largely unknown[2]. As the most well documented biochemical property of p53 is its ability to activate transcription of genes, we examined in detail the transcripts induced by p53 expression before the onset of apoptosis. Of 7,202 transcripts identified, only 14 (0.19%) were found to be markedly increased in p53-expressing cells compared with control cells. Strikingly, many of these genes were predicted to encode proteins that could generate or respond to oxidative stress, including one that is implicated in apoptosis in plant meristems. These observations stimulated additional biochemical and pharmacological experiments suggesting that p53 results in apoptosis through a three-step process: (1) the transcriptional induction of redox-related genes; (2) the formation of reactive oxygen species; and (3) the oxidative degradation of mitochondrial components, culminating in cell death.

To evaluate the patterns of gene expression following p53 expression, we used SAGE, a technique that allows the quantitative evaluation of cellular messenger RNA populations[3]. In brief, the method revolves around short sequence 'tags' (11 base pairs), generated from defined positions within each mRNA molecule. Expression patterns are deduced from the abundance of individual tags. To induce apoptosis, the colorectal cancer line DLD-1, containing an inactive endogenous *p53* gene, was infected with a replication-defective adenovirus encoding p53 (Ad-p53). As previously shown, DLD-1 cells are among the ~50% of colorectal cancer (CRC) lines that undergo apoptosis in response to p53 (ref. 4). RNA was purified from cells 16 h after infection, at least 8 h before the onset of morphological signs of apoptosis.

A total of 101,694 tags were analysed, approximately half from cells infected with Ad-p53 and half from cells infected with a control virus (Ad-lacZ) encoding β-galactosidase. These tags corresponded to 7,202 different transcripts. Comparison of the two SAGE libraries indicated a remarkable similarity in expression profiles (Fig. 1a). Of the 7,202 transcripts detected, only 14 (0.19%) were expressed at levels more than 10-fold greater in p53-expressing than in control cells; conversely, only 20 transcripts were expressed at levels less than 10-fold lower in the p53-expressing cells (see http://welchlink.welch.jhu.edu/~molgen-g/P53-SAGE.HTM). As previous data indicated that p53-mediated transcriptional activation was the likely basis of p53 action[5], we concentrated on the 14 tags appearing at higher levels in the p53-expressing cells. The mRNA transcripts corresponding to 13 of these tags were successfully identified (Table 1), and in each case the induction was confirmed by northern blot analysis (examples shown in Fig. 1b). Only two of these genes (called *PIG*s, for p53-induced genes) had been implicated as targets of p53-transcriptional activation[1,2,5,6], and seven had not previously

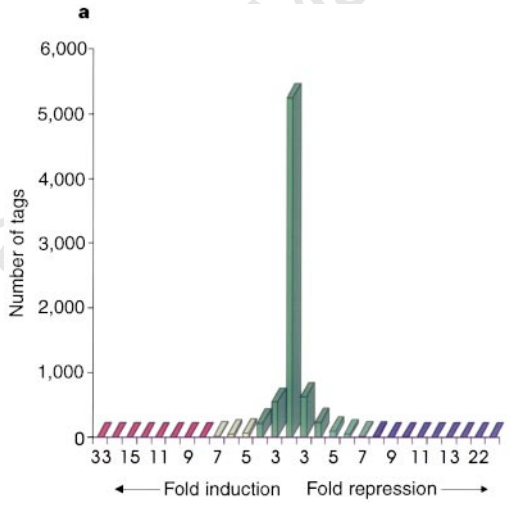

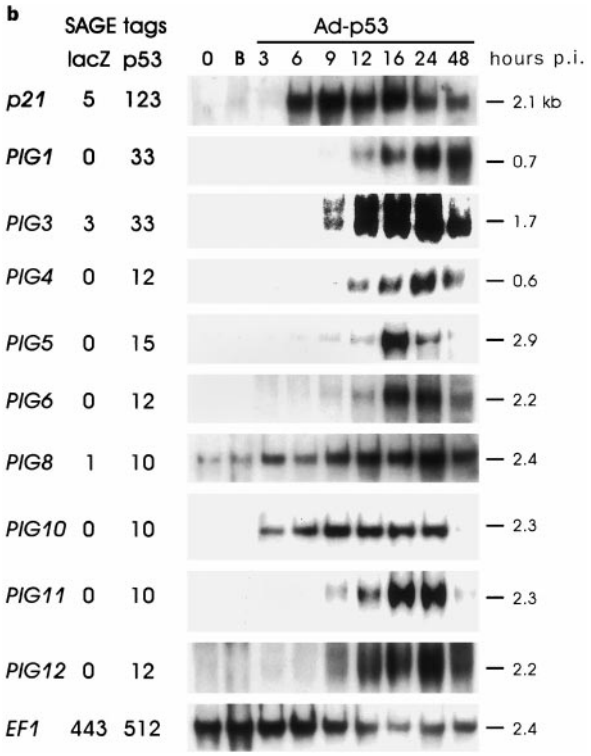

Figure 1 a, Summary of SAGE data. For each of 7,202 different transcripts identified, the ratio of their abundances in the two libraries is plotted. The *y*-axis indicates the number of tags expressed at the ratio indicated on the *x*-axis. Bars representing tags exhibiting less than 5-fold differences in expression are shown in green, and those induced or repressed more than 8-fold are shown in red and blue, respectively. **b**, Northern blot analysis after Ad-p53 infection. Representative northern blots are shown for several transcripts identified by SAGE to be expressed at higher levels in p53-expressing cells at the indicated times post-infection (p.i.). Uninfected cells (column marked zero) and cells infected with Ad-lacZ for 48 h (column marked 'B') were included for comparison. EF1 is a control transcript expressed at relatively equal levels in cells 16 h after infection with Ad-p53 and Ad-lacZ. The SAGE tag abundances (16 h after infection) are included on the left.

been described at all. Other genes previously implicated in p53-mediated responses were induced to lower levels (for example, *MDM2*, thrombospondin) or not at all (for example, *bax* and *cyclin G1*) in the human CRC cells studied here (ref. 4 and http://welchlink.welch.jhu.edu/~molgen-g/P53-SAGE.HTM).

*PIG*s were induced at relatively short times after p53 expression, at least 12 h before any morphological or biochemical signs of apoptosis (Fig. 1b). This suggested that *PIG*s were directly induced by the transcriptional activation properties of p53. To test this conjecture formally in a representative case, we evaluated the genomic structure and sequence of *PIG3*. By screening a bacterial artificial chromosome (BAC) library, a genomic clone was identified that contained all *PIG3* coding sequences. The gene was localized to chromosome 2p (see Methods), and the intron–exon structure and sequence of the promoter region were determined. A 6.1-kilobase (kb) *Apa*LI fragment of genomic DNA containing the presumptive promoter was then cloned upstream of a luciferase reporter gene (Fig. 2a). The resulting construct was transfected into three different human cell lines together with wild-type (WT) or mutant p53. As shown in Fig. 2b, wild-type p53 induced substantial activity through the *PIC3* promoter in all three lines. Mutant p53 had no transcriptional activation capacity. Analysis of a truncated promoter showed that the p53-responsive elements lay within a fragment containing only 862 base pairs (bp) of sequence upstream of the *PIG3* transcription start site (Fig. 2a). Determination of the sequence of the 6.1-kb *Apa*L1 fragment (GenBank accession number AF010317) revealed a single 20-bp sequence predicted to bind p53, located at 308 nucleotides upstream of the transcription start site. A DNA fragment containing two copies of this sequence, but not a derivative of this fragment altered at critical residues, was found to bind strongly to p53 *in vitro* (Fig. 2c). As a further test of the p53-dependence of *PIG3* induction, we determined whether it could be induced by endogenous p53 rather than through the exogenous Ad-p53 source. Six CRC cancer cell lines were each treated with adriamycin, a DNA-damaging and apoptotic-inducing agent known to increase endogenous p53 levels. *PIG3*, like *p21*, was found to be strongly induced in the three lines with wild-type p53 genes, but not in the three lines with mutant *p53* genes (http://welchlink.welch.jhu.edu/~molgen-g/P53-SAGE.HTM).

The sequences of the *PIG*s provided important clues as to their

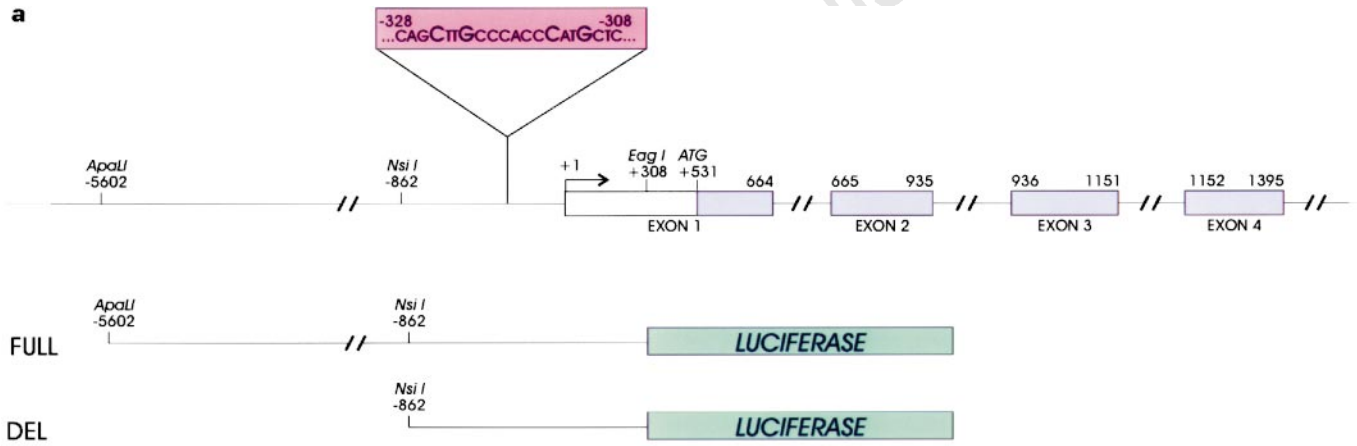

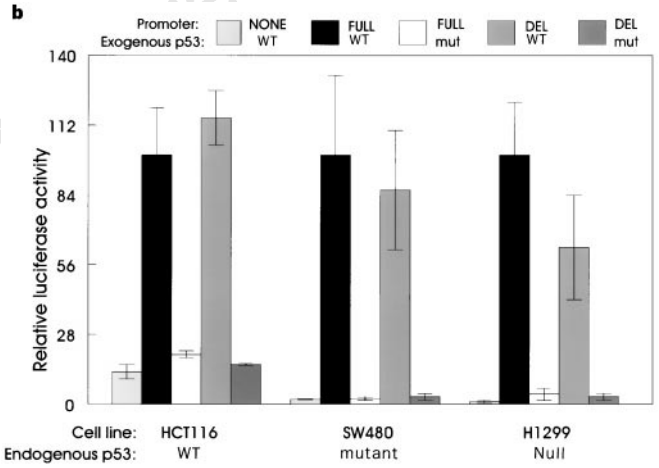

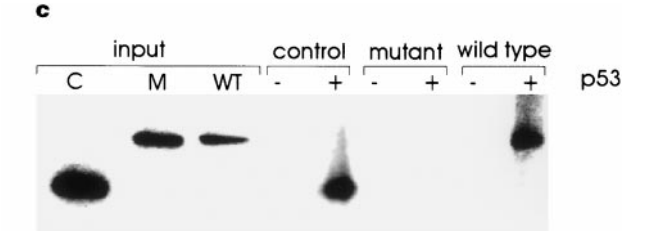

Figure 2 a, The *PIG3* gene, illustrating intron–exon structure and promoter region. Numbers refer to nucleotides relative to the 5′ end of the cDNA. The fragments used for the luciferase constructs had their distal ends at the *Eag*I site within exon 1 and their 5′ ends at either the *Apa*LI or *Nsi*I sites (FULL and DEL, respectively). The p53-binding site located at nt 328–308 is indicated, with upper-case letters corresponding to the highly conserved residues that were altered in one of the oligonucleotides used for immunoprecipitation. **b**, p53 induction of the *PIG3* promoter. Fragments encompassing 5.6 or 0.7 kb (FULL and DEL, respectively) of the *PIG3* gene promoter were cloned upstream of a luciferase reporter and transfected into the indicated cell types in the presence of wild-type (WT) and mutant p53 expression vectors. The levels of luciferase activity were determined in cell lysates 24 h after transfection. **c**, *In vitro* binding assay with end-labelled fragments containing WT and mutant (M) p53 binding sites. A fragment containing thirteen copies of a p53 binding site from the *WAF1* promoter region[26] was used as a control (C). The 'input' lanes contained 0.5% of the amount of fragment used in binding assays.

potential functions (Table 1). In particular, several were predicted to encode proteins with activities related to the redox status of cells. *PIG12* is a novel member of the microsomal glutathione *S*-transferase family of genes (Fig. 3a). *PIG8* is the human homologue of a mouse gene (Ei24) whose expression is induced in a p53-dependent manner by etoposide, a quinone known to generate reactive oxygen species (ROS)[6] (Fig. 3c). *PIG6* is a homologue of proline oxidoreductase (Fig. 3d), a mitochondrial enzyme that catalyses the first step in the conversion of proline to glutamate[7]. Glutamate is one of the three amino acids required for formation of glutathione, a major regulator of cellular redox status. The *p21* gene, which may also be considered to be a *PIG*, can be induced by reactive oxygen species, independently of p53 (ref. 8). *PIG4* encodes a serum amyloid protein that can be induced by oxidative stress[9]. *PIG1* belongs to the galectin family, members of which can stimulate superoxide production[10]. *PIG7* is induced by TNF-α, an inducer of oxidative stress. *PIG3* is a novel gene that is highly related to *TED2*, a plant NADPH oxidoreductase[11] (Fig. 3b). Interestingly, *TED2* is one of the few genes implicated in the apoptotic process necessary for the formation of plant meristems[11]. The closest relative of *PIG3* in mammals is an NADPH–quinone oxidoreductase that is a potent generator of ROS[12].

Reactive oxygen species are powerful inducers of apoptosis[13]. The SAGE-based characterization of p53-induced genes suggested that p53 might induce apoptosis by stimulating the production of ROS. To test this hypothesis, the production of ROS was measured in p53-expressing cells using carboxymethyl dichlorofluorescein diacetate (CM-DCF-DA) and flow cytometry[14]. This analysis showed that ROS were induced following Ad-p53 infection and that ROS continued to increased as apoptotis progressed (Fig. 4a). The magnitude of the increase in ROS, as assessed by CM-DCF-DA fluorescence, was comparable in p53-expressing cells and in cells treated with the powerful oxidant menadione (Fig. 4a). There was no change in CM-DCF-DA fluorescence following infection with a control adenovirus (Fig. 4a). As an assay for the functional consequences of ROS production, we examined the cellular content of cardiolipin, a major component of the mitochondrial membrane which is especially sensitive to cellular oxidation[15]. Using nonyl-acridine orange (NAO) as a probe, cardiolipin was found to decrease soon after p53-induced reactive oxygen species were detected (Fig. 4a), demonstrating significant injury to a major mitochondrial component.

To determine the specificity of *PIG* expression for the p53-dependent apoptotic process, we did experiments with other inducers of ROS or apoptosis. We found that *PIG*s were not expressed simply as a result of ROS production, as none were induced following treatment with menadione and only p21 was induced by hydrogen peroxide in DLD-1 cells (data not shown). Similarly, the specificity of *PIG* induction for p53-dependent apoptosis was confirmed by the demonstration that other inducers of apoptosis (indomethacin or ceramide) did not result in the expression of any *PIG*, despite extensive cell death (data not shown).

To clarify the relationship between p53 expression, *PIG* activation, ROS production, and apoptosis, we carried out more detailed time course experiments. *PIG* induction began within six hours of Ad-53 infection (Figs 1b and 4b), whereas intracellular ROS

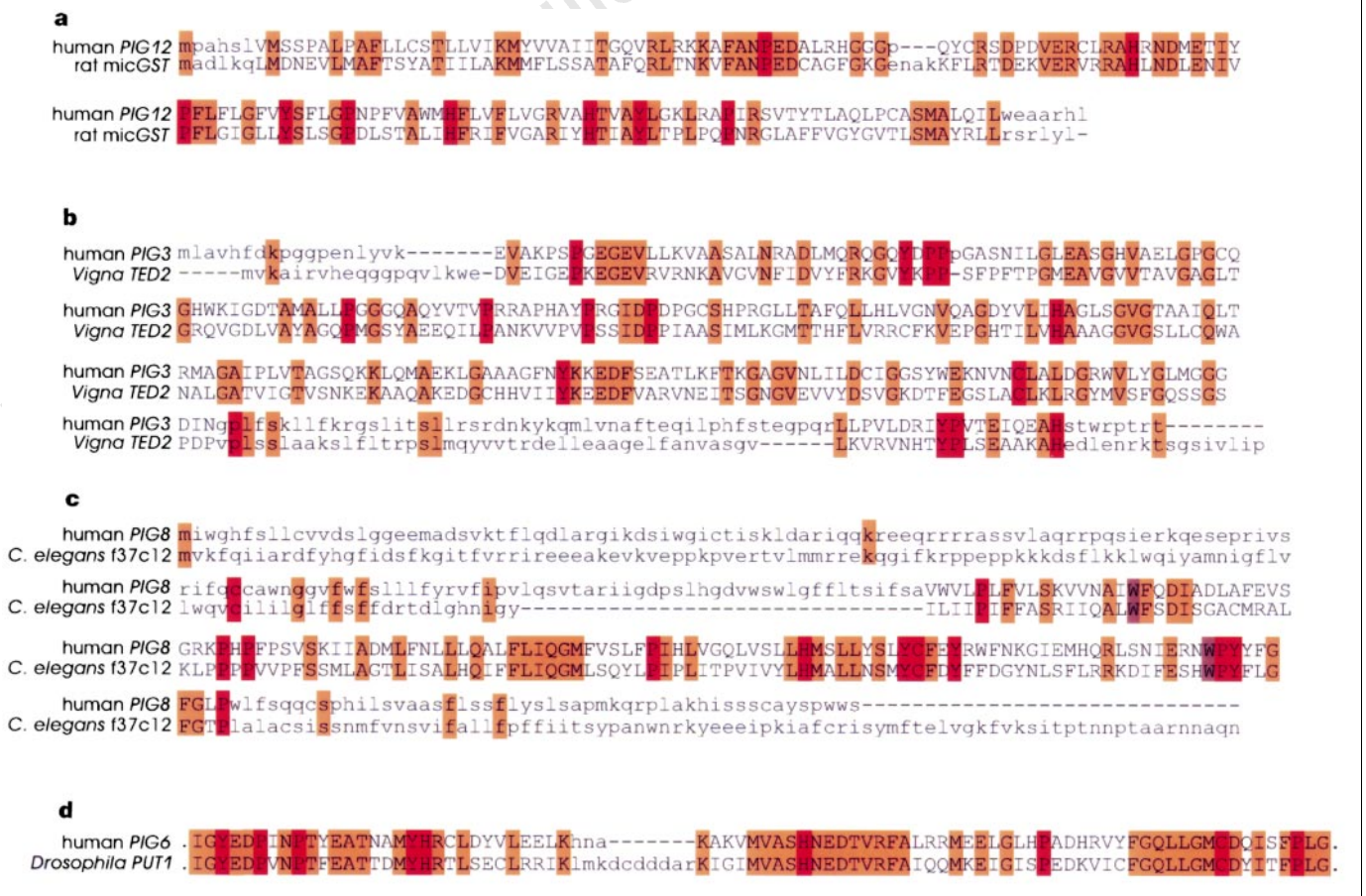

Figure 3 a–c, Sequences of selected genes identified through SAGE. In each case, the indicated gene is compared to the homologue from the non-human species that revealed a clue to its possible function. The amino-acid sequences were aligned using Macaw Version 2.0.3 and are shaded according to the mean of their pairwise scores, with red indicating a higher score than orange. With the exception of *PIG6*, the cloned human sequences appeared to be full-length with respect to the coding region; accession numbers are given in Table 1.

production, as assessed with lucigenin chemiluminescence, could first be observed at 18 h (Fig. 4b). This ROS production led to oxidative stress, as evidenced by a 48 ± 12% decrease in intracellular glutathione concentration at 21 h. Mitochondrial lipid degradation (NAO staining) was not observed until three to six hours after the onset of a measurable ROS increase, and was accompanied by morphological (chromatin condensation and fragmentation) and biochemical (caspase-mediated degradation of polyADP-ribose polymerase (PARP)) signs of apoptosis (Fig. 4b). These observations are consistent with previous studies showing that mitochondrial damage is rapidly followed by classic signs of programmed cell death[13].

The time courses shown in Fig. 4b suggest a cascade in which p53 transcriptionally induces redox-controlling genes, resulting in the production of ROS, in turn leading to oxidative damage to mitochondria and apoptosis. To determine whether these steps are causally associated, we inhibited each of them with specific pharmacological agents and determined the effect of this inhibition on other components of the pathway. First, cells were treated with the transcriptional inhibitor 5,6-dichlorobenimidizole riboside (DRB) at 8 h following Ad-p53 infection[16]. Although p53 expression was already near maximal at this time, DRB was found to block apoptosis at 24 h by 83 ± 3%, as well as to inhibit the expression of *PIG*s. The translational inhibitor cycloheximide, when given up to 8 h following Ad-p53 infection, was found similarly to block apoptosis (by 79% at 24 h). Thus both transcription and translation were required for p53-induced apoptosis in CRC cells, as observed in some other systems and as expected for classic programmed cell death[2,5]. Second, p53-expressing cells were treated with pyrrolidine dithiocarbamate (PDTC), an antioxidant that blocks ROS-associated apoptosis[17]. PDTC was indeed able to block the apoptosis elicited by p53 (data not shown). However, PDTC inhibits many enzymes and its specificity is questionable[17]. We therefore treated cells with diphenyleneiodonium chloride (DPI), a specific inhibitor of flavin-dependent oxidoreductases that has been used to block production of ROS in a variety of systems[18]. Cells were treated with DPI 12 h after Ad-p53 infection, when *PIG* production was already underway, and *PIG3* expression, apoptosis and ROS production were measured 12 h later. DPI (25 μM) did not inhibit *PIG3* production, but inhibited ROS production by 71–85% and inhibited apoptosis by 73–77% in three independent experiments. Finally, we treated cells with bongkrekic acid (BA), a specific inhibitor of mitochondrial ATP translocase which can block the mitochondrial permeability transition pore opening thought to be required for some forms of apoptosis[13]. When cells were treated 12 h after Ad-p53 infection, BA did not inhibit either *PIG3* expression or ROS production, but inhibited subsequent apoptosis by 86–93%. BA was non-toxic at the dose used (100 μM), and although BA inhibited the p53-apoptotic process dependent on ROS production, it had no effect on the p53-mediated growth arrest dependent on p21 (as assessed by flow cytometry).

Our gene-expression profile, time courses, and pharmacological inhibition studies strongly support a three-step model underlying p53's induction of apoptosis. We propose that p53 transcriptionally activates a specific subset of genes, including oxidoreductases, long before any morphological or biochemical evidence of cell death (Table 1 and Fig. 4b). The proteins encoded by these genes then collectively increase the content of ROS, which in turn damage

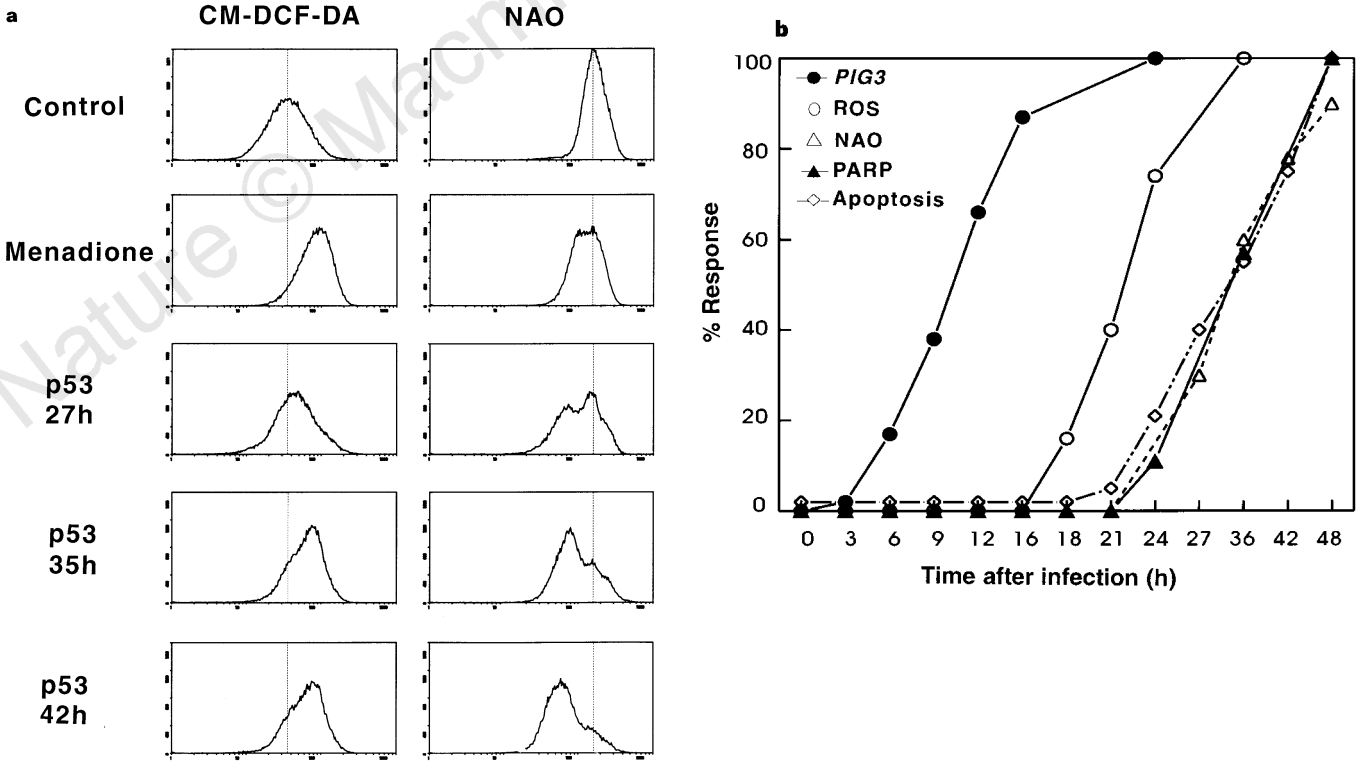

Figure 4 Oxidative stress and mitochondrial damage in p53-mediated apoptosis. **a**, DLD-1 cells were infected with Ad-p53 or control (Ad-lacZ) viruses and collected after 27, 35 or 42 h. Cells were incubated with CM-DCF-DA, a probe of ROS, or NAO, a probe of the mitochondrial membrane cardiolipin, and analysed by flow cytometry. The mean fluorescence of the control cells is indicated by vertical lines in each box. The pro-oxidant drug menadione was used as a positive control to induce oxidative stress. An increase in ROS and a decrease in cardiolipin concentration could be clearly observed by cytometry at 27 h and increased as the p53-expressing cells entered apoptosis. **b**, Time course of apoptosis-related events following p53 expression. Cells were infected with Ad-p53 at 0 hours and *PIG3* expression (●) quantified by densitometry of northern blots. ROS production (○) was assessed with lucigenin; glutathione depletion exhibited a similar time course (not shown). Cardiolipin concentration (△) was assessed with NAO staining. Caspase activation (▲) was assessed by cleavage of PARP, and chromatin condensation/fragmentation (◇) was assessed by staining with DAPI.

Table 1 p53-induced genes (*PIG*s)*

Tag	Name	Function/homology	Accession no.
TGTCCTGGTTC	*p21*	CDK inhibitor	U03106
TAACCTCGTG	*PIG1*	Galectin-7	L07769
CCCTCCTCCGT	*PIG2*	Guanidinoacetate *N*-methyl transferase	Z49878
GAGGCCAACA	*PIG3*	Quinone oxidoreductase homologue	AF010309
GTGCGGAGGAC	*PIG4*	Serum amyloid A	M10906
TGGGGCCGCAG	*PIG5*	Normal keratinocyte mRNA	U33271
TCCTTGGACCT	*PIG6*	Proline oxidase homologue	AF010310
CTGGGCCTGAA	*PIG7*	TNF-α induced mRNA	AF010312
AGCTGGTTTCC	*PIG8*	Etoposide-induced mRNA	AF010313
CGTCCCGGAGC	*PIG9*	Tax1-binding protein	U33822
AGCTCACTCCA	*PIG10*	Actin-binding protein	AF010314
AGGCTGTCCAG	*PIG11*	Unknown	AF010315
TGAGTCCCTGT	*PIG12*	Microsomal glutathione transferase homologue	AF010316
AGATGCTGCAG	*PIG13*	Unknown	NA

* Only those *PIG*s showing tenfold or greater reduction are presented. Additional p53-induced and repressed genes are available through http://welchlink.welch.jhu.edu/~molgen-g/p53-SAGE.HTM.

mitochondria. Leakage of calcium and proteinaceous components from damaged mitochondria then stimulate the caspases that are ubiquitously activated during the apoptotic process[19–22]. Data from several experimental systems are consistent with this model. For example, apoptotis induced by irradiation, which is dependent on p53 in certain cell types, has been proposed to proceed through a process involving ROS and mitochondrial damage[23]. Additionally, an SV40 large-T-antigen mutant, which binds p53 only at the permissive temperature, induces apoptosis at the non-permissive temperature through a ROS-related mechanism[24]. Also, p53-induced apoptosis in smooth-muscle cells is ROS-dependent[25]. Thus, the events we observed in CRC cells are unlikely to be cell-type- or species-specific, and may often underlie p53-associated apoptotic processes. The fact that one of the *PIG*s is highly related to *Ted2*, an oxidoreductase implicated in plant cell apoptosis[11], and that apoptosis in plants may also proceed through a ROS-directed pathway[11], adds further interest to this model.

Although observations by us and others are consistent with this model, they raise several unanswered questions. For example, we do not yet know which of the *PIG*s are primarily responsible for the induction of ROS. We suspect that their combination, rather than any single one, is necessary for ROS generation. This conjecture is supported by preliminary experiments demonstrating that *PIG3* alone does not induce apoptosis when overexpressed (K.P., unpublished data). Although we have concentrated on the most highly induced *PIG*s, the SAGE analysis revealed at least 26 other genes that were induced by p53 to significant but to lower extents than *p21* and *PIG1–PIG13*. Some of these 26 genes (available through http://welchlink.welch. jhu.edu/~molgen-g/P53-SAGE.HTM) may play a role in redox regulation. It is also not known why some cells enter into apoptosis following p53 expression while others undergo a prolonged growth arrest[4]. The possibility that *PIG*s are only induced in the former has been excluded by examination of *PIG* expression in such lines; most *PIG*s were induced by p53 in each of ten CRC lines tested, regardless of whether they underwent apoptosis or growth arrest. A more likely possibility is that different cells have different capacities to cope with generators of oxidative stress, and that cells with a low capacity succumb to apoptosis. This possibility is supported by studies that show that the response to ROS varies significantly with cell type and growth conditions[13]. We hope that the experiments and genes described here will open a new window into the p53 apoptotic process and will facilitate enquiry into these issues. □

Methods

Cells and RNA. All cell lines were obtained from the American Type Culture Collection and were cultured in McCoy's medium supplemented with 10% fetal bovine serum (FBS). Cells were infected with recombinant adenoviruses containing either the *p53* gene or the β-galactosidase gene[26] at a multiplicity of infection of 10–100. RNA was purified from cells at various times after infection, using the MessageMaker Kit (Gibco/BRL). Northern blot analysis has been described[26].

SAGE. SAGE was done as before[3,27]. In brief, polyadenylated RNA was converted to double-stranded cDNA with a BRL synthesis kit following the manufacturer's protocol, with the inclusion of primer biotin-5′-T_{18}-3′. The cDNA was cleaved with *Nla*III and the 3′-terminal cDNA fragments were bound to streptavidin-coated magnetic beads (Dynal). After ligation of oligonucleotides containing recognition sites for *Bsm*FI, the linkered cDNA was released from the beads by digestion with *Bsm*FI. The released tags were ligated to one another, concatemerized, and cloned into the *Sph*I site of pZero 1.0 (Invitrogen). Colonies were screened with PCR using M13 forward and M13 reverse primers. PCR products containing inserts of greater than 300 bp (>20 tags) were sequenced with the TaqFS DyePrimer kit and analysed using a 377 ABI automated sequencer (Perkin Elmer).

Statistical analysis. 53,022 and 51,853 tags were identified from DLD-1 cells infected with Ad-p53 and Ad-lacZ, respectively. The two libraries were compared using the SAGE program group[3]. Corrections for tags containing linker sequences and other potential artefacts were made as described[27]. Of 104,875 total tags identified, 3,181 were excluded from analysis on this basis. Monte Carlo simulations revealed that the computational analyses had a >99% probability of detecting a transcript expressed at an abundance of 0.00005 in either RNA sample.

cDNA clones. Cellular mRNA from Ad-p53-infected cells was used to prepare cDNA as described for the SAGE libraries except that the 3′ primer contained an additional M13 forward sequence between the oligo(dT) tract and the biotinylated 5′ residue. To determine the sequence of the transcript from which an individual tag was derived, this cDNA was used as a template for PCR, employing an M13 forward primer and a primer containing the tag sequence. In other cases, mRNA from Ad-p53-infected cells was used to construct a cDNA library in the ZAP Express vector (Stratagene) and the library was screened by hybridization with oligonucleotides corresponding to tags, as described[3]. Of 14 tags identified by SAGE as differentially expressed in p53-expressing cells, 8 corresponding genes could be identified simply by searching public databases, particularly those including expressed sequence tags. In 5 cases, one of the two strategies described was used to obtain the corresponding *PIG*. In one of the 14 cases (*PIG13*), no cDNA clone could be recovered corresponding to the tag sequence.

Analysis of *PIG3* genomic structure. An arrayed BAC library (Research Genetics) was screened by PCR using the following primers derived from the 5′ end of the *PIG3* gene: 5′-ggc-cag-gag-taa-gta-act-3′ and 5′-gcc-ctg-gtc-tgc-cgc-gga-3′. *Eco*RI fragments encompassing the *PIG3* coding sequences were subcloned into pBR322 and partially sequenced to determine the intron–exon borders. A 6.1-kb *Apa*LI fragment whose 3′ end was at a *Eag*I site 308 bp downstream of the transcription start site was then cloned into a promoterless luciferase reporter vector (Fig. 2a). This fragment was completely sequenced by primer walking. Subclones were then generated by restriction endonuclease digestion. Luciferase activity was determined after co-transfection with expression vectors encoding wild-type or R175H mutant p53. For *in vitro* p53 binding experiments, oligonucleotides containing two copies of the predicted p53-binding site (Fig. 2a) were subcloned into a modified pBR322 vector, excised as

a ~260-bp restriction fragment, and end-labelled. Immunochemical assays were performed as described[28].

Flow cytometry and other assays. Cells were collected with the aid of trypsin and incubated with CM-DCF-DA or NAO (Molecular Probes) at concentrations of 10 and 0.4 μM, respectively, for 20 min at 37C before analysis by flow cytometry[14,15]. To determine the fraction of apoptotic cells after various treatments, cells were stained with the DNA-binding dye H33258 and evaluated by fluorescence microscopy or flow cytometry as described[1]. Superoxide production was assessed with lucigenin[29]. In brief, $4–5 \times 10^6$ cells were collected with a rubber policeman and resuspended in 1 ml Earle's balanced salt solution (Life Technologies). Dark-adapted lucigenin (bis-*N*-methylacridinium nitrate; Sigma) was added to the samples to 20 μM final concentration. Light emission was detected using a Berthold LB 9505 luminometer for 60 min at 37 °C. Glutathione concentrations were measured using an assay kit (Oxford Biomedical) according to the manufacturer's instructions. Caspase activation was assessed by cleavage of PARP. Lysates from cells infected with Ad-p53 were western-blotted with an anti-PARP antibody and the cleavage fragments quantified by densitometry[4].

Received 27 May; accepted 1 July 1997.

1. Waldman, T., Kinzler, K. W. & Vogelstein, B. p21 is necessary for the p53-mediated G1 arrest in human cancer cells. *Cancer Res.* **55,** 5187–5190 (1995).
2. Oren, M. Relationship of p53 to the control of apoptotic cell death. *Semin. Cancer Biol.* **5,** 221–227 (1994).
3. Velculescu, V. E., Zhang, L., Vogelstein, B. & Kinzler, K. W. Serial analysis of gene expression. *Science* **270,** 484–487 (1995).
4. Polyak, K., Walkman, T., He, T.-C., Kinzler, K. W. & Vogelstein, B. Genetic determinants of p53 induced apoptosis and growth arrest. *Genes Dev.* **10,** 1945–1952 (1966).
5. Levine, A. J. p53, the cellular gatekeeper for growth and division. *Cell* **88,** 323–331 (1997).
6. Lehar, S. M. *et al.* Identification and cloning of Ei24, a gene induced by p53 in etoposide-treated cells. *Oncogene* **12,** 1181–1187 (1996).
7. Hayward, D. C. *et al.* The *sluggish-A* gene of *Drosophila melanogaster* is expressed in the nervous system and encodes proline oxidase, a mitochondrial enzyme involved in glutamate biosynthesis. *Proc. Natl Acad. Sci. USA* **90,** 2979–2983 (1993).
8. Russo, T. *et al.* A p53-independent pathway for activation of WAF1/CIP1 expression following oxidative stress. *J. Biol. Chem.* **270,** 29386–29391 (1995).
9. Reinhoff, H. Y. Jr, Huang, J. H., Li, X. X. & Liao, W. S. Molecular and cellular biology of serum amyloid A. *Mol. Biol. Med.* **7,** 287–298 (1990).
10. Yamaoka, A., Kuwabara, I., Frigeri, I. G. & Liu, F. T. A human lectin, galectin-3 (epsilon bp/Mac-2) stimulates superoxide production by neutrophils. *J. Immunol.* **154,** 3479–3487 (1995).
11. Greenberg, J. T. Programmed cell death: A way of life for plants. *Proc. Natl Acad. Sci. USA* **93,** 12094–12097 (1996).
12. Rao, P. V., Krishna, C. M. & Zigler, J. S. Jr Identification and characterization of the enzymatic activity of zeta-crystallin from guinea *PIG* lens. A novel NADPH : quinone oxidoreductase. *J. Biol. Chem.* **267,** 96–102 (1992).
13. Kroemer, G., Zamzami, N. & Susin, S. A. Mitochondrial control of apoptosis. *Immun. Today* **18,** 45–51 (1997).
14. Zamzami, N. *et al.* Reduction in mitochondrial potential constitutes an early irreversible step of programmed lymphocyte death *in vivo*. *J. Exp. Med.* **181,** 1661–1672 (1995).
15. Petit, P. X. *et al.* Alterations in mitochondrial structure and function are early events of dexamethasone-induced thymocyte apoptosis. *J. Cell. Biol.* **130,** 157–167 (1995).
16. Tamm, I. & Sehgal, P. B. Halobenzimidazole ribosides and RNA synthesis of cells and viruses. *Adv. Virus Res.* **22,** 187–258 (1978).
17. Orrenius, S., Nobel, C. S. I., van den Dobbelsteen, D. J., Burkitt, M. J. & Slater, A. F. G. Dithiocarbamates and the redox regulation of cell death. *Biochem. Soc. Transact.* **24,** 1032–1038 (1996).
18. Holland, P. C., Clark, M. G., Bloxham, D. P. & Lardy, H. A. Mechanism of action of the hypoglycemic agent diphenyleneiodonium. *J. Biol. Chem.* **248,** 6050–6056 (1973).
19. Korsmeyer, S. J. Regulators of cell death. *Trends Genet.* **11,** 101–105 (1995).
20. Susin, S. A. *et al.* Bcl-2 inhibits the mitochondrial release of an apoptogenic protease. *J. Exp. Med.* **184,** 1331–1341 (1996).
21. Yang, J. *et al.* Prevention of apoptosis by Bcl-2: release of cytochrome *c* from mitochondria blocked. *Science* **275,** 1129–1132 (1997).
22. Kluck, R. M., Bossy-Wetzel, E., Green, D. R. & Newmeyer, D. D. The release of cytochrome *c* from mitochondria: a primary site for Bcl-2 regulation of apoptosis. *Science* **275,** 1132–1136 (1997).
23. Borek, C. Radiation and chemically induced transformation: free radicals, antioxidants and cancer. *Br. J. Cancer suppl.* **8,** 74–86 (1987).
24. Vayssiere, J. L., Petit, P. X., Risler, Y. & Mignotte, B. Commitment to apoptosis is associated with changes in mitochondrial biogenesis and activity in cell lines conditionally immortalized with simian virus 40. *Proc. Natl Acad. Sci. USA* **91,** 11752–11756 (1994).
25. Johnson, T. M., Yu, Z.-X., Ferrans, V. J., Lowenstein, R. A. & Finkel, T. Reactive oxygen species are downstream mediators of p53-dependent apoptosis. *Proc. Natl Acad. Sci. USA* **93,** 11848–11852 (1996).
26. El-Diery, W. S. *et al.* WAF1, a potential mediator of p53 tumor suppression. *Cell* **75,** 817–825 (1993).
27. Velculescu, V. E. *et al.* Characterization of the yeast transcriptome. *Cell* **88,** 243–251 (1997).
28. El-Deiry, W. S., Kern, S. E., Pietenpol, J. A., Kinzler, K. W. & Vogelstein, B. Definition of a consensus binding site for p53. *Nature Genet.* **1,** 45–49 (1992).
29. Faulkner, K. & Fridovich, I. Luminol and lucigenin as detectors for O_2^-. *Free Rad. Biol. Med.* **15,** 447–451 (1993).

Acknowledgements. We thank V. Velculescu, L. Zhang and W. Zhou for help with SAGE analysis; J. A. Duine for bongkrekic acid; J. Flook for assistance with flow cytometry; and members of our laboratories for discussion. This work was supported by the Clayton Fund and by grants from the NIH. K.P. is a research associate and B.V. is an investigator of the Howard Hughes Medical Institute.

Correspondence and requests for materials should be addressed to K.W.K.

Self-organization of microtubules and motors

F. J. Nédélec*†, T. Surrey*, A. C. Maggs† & S. Leibler*

** Departments of Molecular Biology and Physics, Princeton Unviersity, Princeton, New Jersey 08544, USA*
Laboratoire de Physico-Chimie Théorique, Ecole Supérieure de Physique et Chimie Industrielles, 10 rue Vauquelin, 75231 Paris, France

Cellular structures are established and maintained through a dynamic interplay between assembly and regulatory processes. Self-organization of molecular components provides a variety of possible spatial structures: the regulatory machinery chooses the most appropriate to express a given cellular function[1]. Here we study the extent and the characteristics of self-organization using microtubules and molecular motors[2] as a model system. These components are known to participate in the formation of many cellular structures, such as the dynamic asters found in mitotic and meiotic spindles[3,4]. Purified motors and microtubules have previously been observed to form asters *in vitro*[5]. We have reproduced this result with a simple system consisting solely of multi-headed constructs of the motor protein kinesin[6] and stabilized microtubules. We show that dynamic asters can also be obtained from a homogeneous solution of tubulin and motors. By varying the relative concentrations of the components, we obtain a variety of self-organized structures. Further, by studying this process in a constrained geometry of micro-fabricated glass chambers[7], we demonstrate that the same final structure can be reached through different assembly 'pathways'.

A dividing cell has to separate spatially its newly duplicated chromosomes. It uses the bipolar spindle, a complex molecular structure made of many different protein components, to accomplish this task with high precision. Spindle formation is an intensively studied prototype of cell morphogenesis phenomena. A bipolar spindle forms when mitotic chromosomes capture and selectively stabilize dynamic microtubules nucleated by two centrosomes[1]. This assembly process tolerates numerous variations in intermediate configurations, such as different chromosome positions and geometrical and mechanical perturbations[8]. Spindles

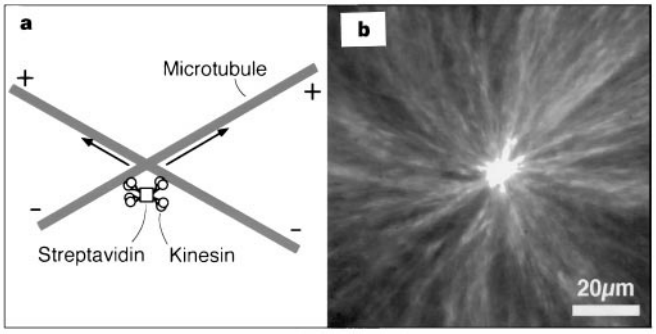

Figure 1 Self-organization of taxol-stabilized microtubules and kinesin constructs into asters. **a**, Schematic representation of a kinesin–streptavidin construct moving simultaneously along two microtubules. The kinesin constructs can be seen as force-generating, mobile crosslinks. **b**, A self-organized aster observed by dark-field microscopy. Polymerized and taxol-stabilized microtubules were mixed with motor constructs and ATP. The sample is shown after ~2 min. The bright spot in the centre of the aster is caused by light scattering from accumulated microtubules and motors. In cells and cell-free extracts, where the asters are organized by minus-end directed motors such as dyneins[16,17], the aster polarity is opposite. Scale bar, 20 μm.